The Astrophysical Journal, 964:112 (11pp), 2024 April 1 https://doi.org/10.3847/1538-4357/ad2520

Exploring Spatial and Temporal Patterns in the Debrecen Solar Faculae Database: Part I

Anett Elek[1,2], Marianna B. Korsós[2,3,4], Mausumi Dikpati[5], Norbert G. Gyenge[2,6], Bernadett Belucz[2,6], and Robertus Erdélyi[2,4,6]
[1] University of Debrecen, Egyetem tér 1, H-4032 Debrecen, Hungary
[2] Hungarian Solar Physics Foundation, Petőfi tér 3, H-5700 Gyula, Hungary; komabi@gmail.com
[3] Dipartimento di Fisica e Astronomia "Ettore Majorana," Università di Catania, Via S. Sofia 78, I 95123 Catania, Italy
[4] Department of Astronomy, Eötvös Loránd University, Pázmány Péter sétány 1/A, H-1112 Budapest, Hungary
[5] High Altitude Observatory, NCAR, 3080 Center Green Drive, Boulder, CO 80301, USA
[6] Solar Physics and Space Plasma Research Center, School of Mathematics and Statistics, University of Sheffield, S3 7RH, UK
Received 2023 October 9; revised 2024 January 17; accepted 2024 January 28; published 2024 March 21

Abstract

Photospheric faculae are markers of the solar magnetic field, appearing as bright regions along the edges of granules on the Sun's surface. Using data from the Debrecen Solar Faculae Database, we investigated the spatiotemporal distribution of photospheric faculae between 2010 May 1 and 2014 December 31 and found the following. (i) At lower latitudes, there is an enhanced abundance of faculae appearing as stripes at given Carrington longitudes, which are interpreted as indicative of the presence of active longitudes. (ii) At higher latitudes, we identified so-called crisscross patterns of facular appearance. These patterns are likely the result of faculae in regions situated along the boundaries of supergranules. Last but not least, (iii) various periods of oscillatory phenomena were identified in this facular data set, including a longer periodic range consistent with the quasi-biennial oscillations and shorter ones with periods of 4–12 days. Our findings are supported by the visualization of a simple heuristic thought experiment and more complex dynamo simulations, strengthening the proposed interpretation of the three observed solar phenomena reported.

Unified Astronomy Thesaurus concepts: Solar faculae (1494)

Supporting material: animation

1. Motivation

Analyzing how the properties of various small-scale, short-lived, localized solar phenomena may change over longer timescales, e.g., comparable to that of the solar cycle evolution, can help us to obtain a better grasp of solar activity. Among such important spatiotemporally localized markers of our active Sun are the solar faculae abundantly present at the visible surface of the Sun. The average size of a facula is 100 km (Berger et al. 2007). These faculae are characterized as bright spots in the photosphere that should not be mistaken for chromospheric plage, often referred to as chromospheric faculae. In our present work, we only focus on photospheric faculae, and we refer to them simply as faculae hereafter.

Several models have been introduced to elucidate the observed characteristics of faculae, which encompass broad-spectrum emissions at temperatures exceeding the Sun's effective temperature, their correlation with the near-subsurface magnetic flux elements, and their brightness modulation based on their proximity to the center of the solar disk (Hale 1922). For instance, the application of the "hot wall" model indicates that faculae are local depressions within the photosphere, formed due to the accumulation of magnetic flux. Therefore, faculae shine brightly due to the heightened temperature of the surrounding wall of this depression (Spruit 1976, 1977; Keller et al. 2004).

In general, two types of solar photospheric faculae may be distinguished. The first type represents faculae at the lower latitudes. One notable characteristic of these lower-latitude faculae is the negative correlation between the area of the sunspot and the facular-to-sunspot-area ratio (Chapman et al. 1997). Similar findings were reported by Foukal (1998) and Shapiro et al. (2014) through analyzing data over multiple solar cycles. The relationship between faculae and sunspots is rather intricate because the presence of faculae at a specific time is not solely determined by the concurrent existence of sunspots. Active regions and their remnants as a whole decay more slowly than the individual sunspots they initially harbored. Consequently, the magnetic flux from a particular active region persists, giving rise to faculae even after the sunspots within it have faded away (van Driel-Gesztelyi & Green 2015). The latter implies that, at any given moment of time, there can be faculae structures present that are directly associated not with the currently visible sunspot-bearing active regions, but rather with previous active regions where the sunspots have already dissipated.

The second group of faculae appear at high latitudes, near the solar poles in both hemispheres, generally above $|\pm 70^{\circ}|$ Carrington latitudes. The magnetic field polarity within polar faculae tends to coincide with that of the prevailing polar magnetic field, as discussed by, e.g., Homann et al. (1997). Further studies have demonstrated a correlation between the presence of polar faculae and the strength of the polar magnetic field (Sheeley 1991, 2008; Muñoz-Jaramillo et al. 2012). This relationship has also been characterized as a predictive indicator of the amplitude of the subsequent sunspot cycle in many cases (Tlatov 2009; Priyal et al. 2014; Janssens 2021).

Besides the spatial distribution and magnetic flux of faculae, the life expectancy of these solar photospheric features is also an established topic for research. There is a consensus in

several studies that larger faculae tend to have a longer lifetime (Hirayama 1978). Overall, the lifetime of faculae can range from a few minutes to several hours. Smaller ones may last only up to 16 minutes (Hirayama 1978; Solov'ev & Kirichek 2019). Larger faculae of around 2″ in size can persist for 3–5 hr (Hirayama 1978), while polar faculae have an even longer lifespan of 5–6 hr (Hovis-Afflerbach & Pesnell 2022).

The abovementioned studies helped our understanding of the dynamics of solar faculae, which has become a more popular topic since a number of investigations successfully connected solar faculae with the global properties of the Sun. For example, a relationship was found between faculae and the solar cycle evolution (Janssens 2021). Such a relationship is intriguing because faculae also significantly contribute to solar irradiance (Foukal & Lean 1986). The fluctuation in solar irradiance over timescales exceeding a day is primarily attributed to photospheric magnetism (Walton et al. 2003; Yeo et al. 2017). Models have been developed to capture this variability in solar irradiance by establishing a connection with magnetic activity on the solar surface, supplying the necessary radiative forcing input even for climate simulations (Haigh 2007). Solar irradiance variability is typically represented as the combined impact of diminished intensity due to sunspots and augmented radiance from faculae (Yeo et al. 2014). Such studies overwhelmingly support the conjecture that a "highly localized," i.e., small-scale, but ubiquitous solar phenomenon like the solar faculae can be a dominant contributing element in the understanding of the global behavior of our Sun. This latter aspect is now a strong motivation for the present work to examine the spatiotemporal distribution of the highly localized faculae and their general migration—as markers or tracers of the global solar activity (e.g., global magnetic field evolution)—across the solar disk.

While dynamo theory has made vast progress over the past 70 yr, since the first solar dynamo theory by Parker (1955), as of today the focus is on reproducing a solar-like butterfly diagram by generating a toroidal field that migrates toward the equator with time and reverses after ∼11 yr. Parker (1955) also proposed that the spot-producing fields are essentially the dynamo-generated toroidal fields, which emerge on the surface from the deeper-down dynamo layer by magnetic buoyancy and produce tilted bipolar spots. The 2D (latitude-radius) mean-field kinematic flux-transport dynamos, which operate under the advective-diffusive mechanism so that a meridional circulation along with turbulent diffusion play crucial roles, were considered to be successful in simulating many solar cycle features, including the correct phase relationship between the strong spot-producing toroidal fields and weak polar fields, namely, the polar field changing sign from positive to negative when subsurface toroidal fields have already been negative (Dikpati & Charbonneau 1999; Belucz et al. 2015). Despite these successes, 2D axisymmetric dynamos obviously cannot reproduce 3D (longitude-dependent) solar cycle features, namely, nearly systematic longitude distributions of active regions, sector boundary structures, and evolution of coronal holes. On the other hand, full 3D convective dynamo models have made enormous progress in simulating 3D dynamo action along with irregularly cyclic field reversal (Charbonneau 2020). However, neither the 2D mean-field dynamos nor the full 3D convective dynamos are able to simulate the aforementioned 3D solar cycle features. More importantly, apart from specific longitude distributions of active regions' emergence, it has long been observed that active regions prefer to emerge at the same longitudes where there were already previous emergences (Benevolenskaya et al. 1999; Mandal et al. 2017; Ruždjak et al. 2023). These persistent longitude locations are named as active longitudes (ALs).

So far, dynamo models that can simulate either the longitude distribution of active regions or the persistence of longitudes where activity recurs for several Carrington rotations are still lacking. There has been progress on the physical understanding though. Separate global dynamical processes operating on the dynamo-generated axisymmetric toroidal field can create such preferences of longitudes for active regions' emergence. Interaction among differential rotation, Rossby waves, and toroidal fields can create preferred longitudes in one or more locations that persist for several Carrington rotations (see, e.g., Figure 12 of Dikpati & McIntosh 2020). Therefore, simulating the global distribution of active regions on the Sun, as well as recurrence of active region's emergence at certain longitudes can be considered as essential components of a 3D dynamo, or the processes that operate separately on the dynamo-generated axisymmetric toroidal field. The latter is already well established, but the former remains a challenge for 3D dynamo models, namely, whether a 3D solar dynamo model can be built that would simulate not only the longitude-averaged butterfly diagram but also longitude-dependent solar cycle features, such as ALs. The ALs are also often called "active nests" (Castenmiller et al. 1986; de Toma et al. 2000), which tend to reappear at a consistent longitude during subsequent 27.3 day Carrington rotations (de Toma et al. 2000). These AL bands are approximately 20°–60° wide (Bumba & Howard 1969; Gyenge et al. 2014). Gaizauskas et al. (1983) stated that complexes of solar activity on these ALs are sustained by the frequent emergence of new magnetic fluxes. There is still debate about the presence of ALs in the literature. The stakes are high, as the proven presence of ALs may challenge dynamo theory.

In this work, we only report the observed findings, with some initial theoretical support. The paper is organized as follows. In Section 2, we introduce the facular database that we use, and we outline our data processing method to provide the background to our analysis. Sections 3 and 4 detail our data analysis and the observed findings. Section 5 discusses a simple MHD model that supports these findings and the results. In Section 6, different oscillations of the loci of facular tracers are unveiled to further support the results of Sections 3–5. Section 7 summarizes our conclusions.

2. Collecting Observational Data

The present work concentrates on the spatial and temporal variation of the photospheric faculae. For such an investigation, a very suitable database is the Debrecen Faculae Data Catalogue (Baranyi et al. 2016), which has two subsets of detailed faculae data sets. The first data set is derived from measurements made by the Michelson Doppler Imager (MDI) on board the Solar and Heliospheric Observatory (SOHO). These data cover the period ranging from 1996 to 2010 and are called the SOHO/MDI-Debrecen Faculae Data Catalogue (SDD). The second data set is based on observations from the Helioseismic and Magnetic Imager (HMI) on board the Solar Dynamics Observatory (SDO). This data set spans from 2010 to 2015 and is known as the SDO/HMI-Debrecen Faculae Data Catalogue (HMIDD). These two catalogs with

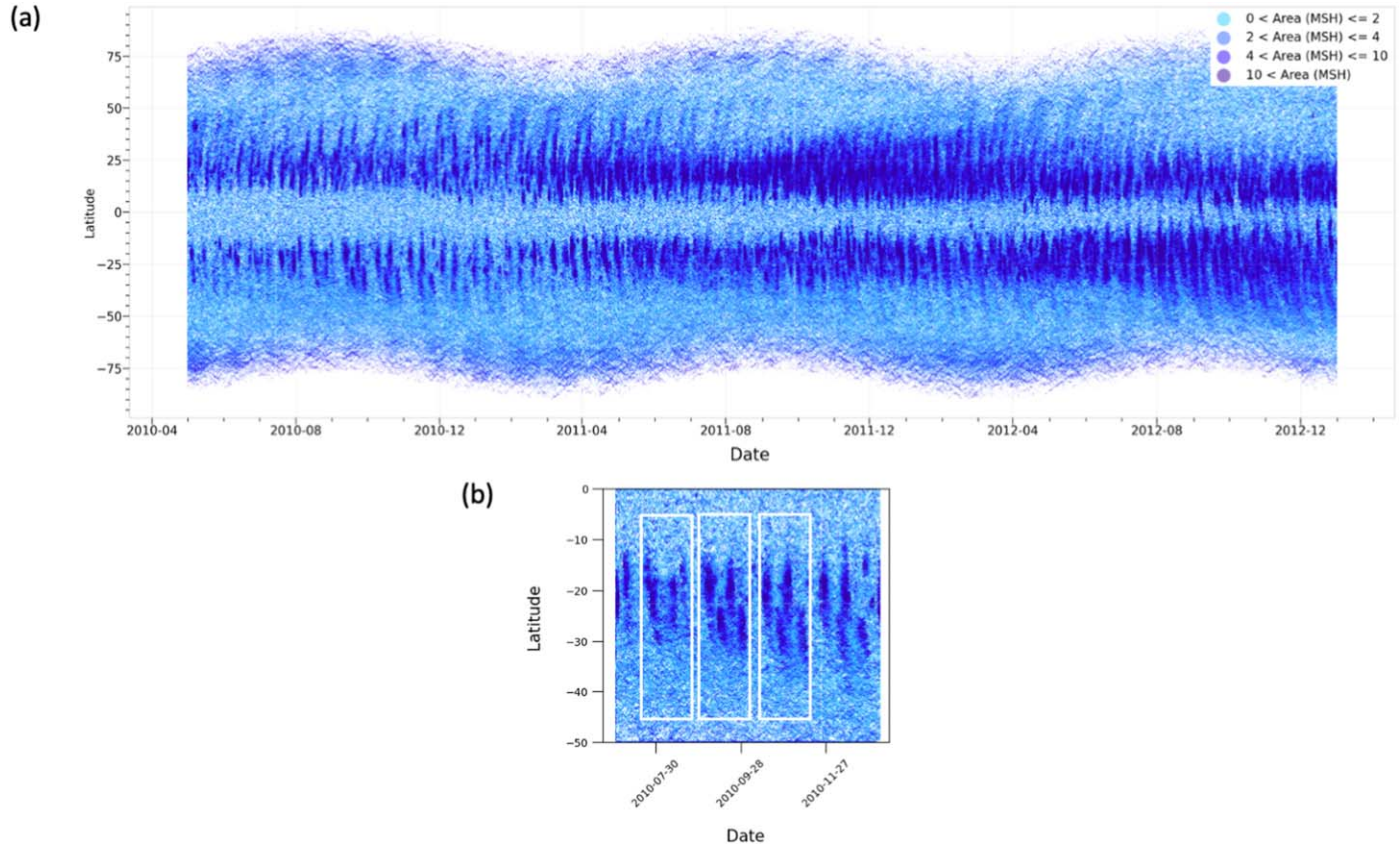

Figure 1. Spatiotemporal evolution of faculae based on data from the HMIDD catalog. Panel (a): the *x*-axis shows the investigated time period between 2010 May 1 and 2014 December 31. The *y*-axis represents the latitude of the faculae. Data displayed are based on the area of the faculae. Lighter spots are smaller and darker (deepest blue) ones are bigger—over 10 MSH (for value bands, see the inset). Note that the dark blue parts between about 10° and 40° are due not to larger size but rather to the higher number of small faculae displayed close to each other. Panel (b): magnified part from panel (a) between 2010 June 10 and 2010 September 8, where one can see much closer how the stripes, representing concurrent abundance, appear periodically. The white squares highlight some of the dual-stripe bands.

space-based observations are essential because they provide important magnetic field information for a wide range of faculae. The cadence of the SDD is 1.5 hr, whereas the cadence of the HMIDD is 1 hr. The spatial resolution of HMIDD is greater than that of SDD, owing to the differences in spatial resolution between the HMI, which has 4096×4096 pixels, and the MDI, with 1024×1024 pixels. Each entry of these two catalogs includes parameters like the date and time of observation, the number of faculae on the solar disk, the size of each facula, their positions on the Sun, and the average magnetic field value within a given facular area.

While the SDD and HMIDD catalogs are similar in nature, there is a slight and important difference because HMI has a higher spatial resolution than MDI. So, to keep our data set consistent, we now only focus on the data from the HMIDD catalog between 2010 May 1 and 2014 December 31. Unfortunately, the HMIDD catalog was stopped because the Debrecen Heliophysical Observatory was shut down due to a shortage of funding. For exploring the spatial and temporal patterns of the photospheric faculae, however, the HMIDD catalog is well suited, as it contains the necessary details.

For the current study, we left out those faculae that were too close to the edge of the visible disk of the Sun (i.e., where the longitudinal distance from the Sun's central meridian, LCM, is over $|70|$) to maintain the quality of the reconstruction of the magnetic field values and reduce uncertainties caused by the line-of-sight effects. Additionally, we have also not included faculae with extremely high magnetic field strengths. Therefore, our study focuses on faculae that have a longitude $-70 <$ LCM $< 70°$ with magnetic field strengths between -500 and 500 G. The $|500|$ G was chosen as the upper limit for the magnetic field value of the faculae because these regions typically have a spatially averaged field strength up to $|500|$ G (Frazier 1971; Title et al. 1992). They consist of magnetic elements of various sizes, interspersed with comparatively field-free or weak-field gas.

3. Spatial Properties of Solar Faculae

In Figure 1, we show the evolution of loci of solar faculae as tracers of a localized enhanced magnetic field along the latitude direction between 2010 May 1 and 2014 December 31. Here, the data are sampled every 2 hr, and the colors used (see the color code inset) correspond to the area size of the faculae. Light blue hues represent smaller faculae (under 2 millionths of the solar hemisphere, MSH), while dark blue shades indicate larger ones. The periodic fluctuations observed at very high latitudes, a sort of sinusoidal envelope, are attributed to the 7° angle between the solar equator and ecliptics (Győri 2012). Such an envelope is the geometric consequence of the varying annual observing angle of the satellites that take the observations (e.g., SDO or SOHO).

Upon carefully examining Figure 1(a), we noticed certain alternating, vertically aligned stripes within the active belt from $-50°$ to 50°. These alternating stripes form dual stripes that are more evident in the white squares in Figure 1(b), as it is a

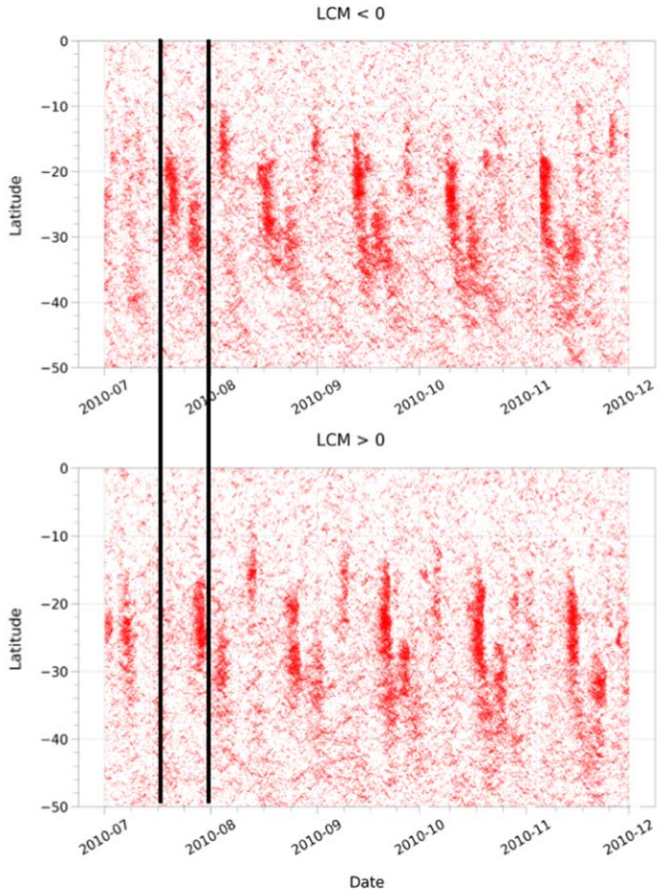

Figure 2. Shift between the faculae data observed separately at two solar disk limbs. Faculae time-space distribution 2010 July–December, with a sampling frequency of 2 hr. The displayed faculae have a magnetic field of 0–500 G and can be found between latitudes of the southern hemisphere between 0° and 50°. In the upper figure, there are faculae at the eastern side of the solar disk (left from LCM = 0), and below there is a panel with faculae detected at the western side of the disk (right from LCM = 0). The first black line marks a stripe of faculae, or a pair of faculae stripes, at the left side of the solar disk (upper image). The second black line marks the progression of this stripe on the right side of the solar disk. The time difference between the two lines is about 10 days. This can be easily calculated since the minor locator on the *x*-axis has a step size of 7 days.

zoomed-in view of the time period between 2010 July 1 and 2010 December 1. To further investigate these stripes, we separately examined their appearance on the east (LCM < 0) and west (LCM > 0) sides. If we consider the spatial and temporal evolution of the faculae on the two sides, as depicted in Figure 2, then we can observe a $\sim$10 day shift between succeeding pairs of stripes on the east and west sides. One of the 10 day shift intervals is visualized by the two black vertical lines in Figure 2, where we can see that the stripe pairs are shifted by about 10 days when comparing their locations in the eastern and western hemispheres between the two black vertical lines. If the stripes correspond to the AL phenomenon, then the 10 day period is consistent with the time required for an active region on the AL to travel from LCM $= -70$ to LCM $= +70$ due to differential rotation.

The feature found is because we observe the solar faculae only around the solar limb regions in a narrow observing window on the west and east, measured from the LMC = 0. Therefore, the 10 day interval between consecutive stripes corresponds to the solar angular rotation speed. These alternated stripes are here proposed to be interpreted as the consequence of the presence of ALs. The AL is identified by the longitudinal nonhomogeneous spatial distribution of sunspot groups (Gyenge et al. 2017). When the photospheric faculae tend to concentrate around sunspot groups, faculae also could show similar features (Elek et al. 2017). To further support the connection between the observed stripe features based on the spatial distribution of faculae and the AL, we prepared a synthetic facular distribution model, visualized by a cartoon; see Figure 3. Here, faculae are randomly scattered across the solar disk. However, around two longitudes about 180° apart, the surface density of these synthetic faculae is artificially enhanced. This visualization is further complemented by the Figure 3 animation that illustrates the presence of this pair of ALs while the Sun rotates and how one would observe them with a narrow observing window in the longitudinal direction. The visualization model of the synthetic AL is then constructed based on the following assumptions.

1. The randomly distributed faculae are detected only with a narrow observing window close to the solar limbs to capture the selection of observations made by the SDO satellite.
2. Faculae tend to be enhanced near two ALs. The second AL (i.e., "behind") is 180° longitude from the one in the front; see Gyenge et al. (2016).
3. The latitudinal distribution of solar faculae follows the latitudinal migration of sunspot groups over decade timescales; i.e., solar faculae follow the butterfly diagram.
4. Faculae with loci that appear along the boundaries of supergranules follow the local horizontal flow field.
5. The ratio between the number of synthetic faculae around the AL and the randomly distributed aggregated faculae number elsewhere can be varied. Depending on its value, we refer to this ratio as high and low noise signal ratio hereinafter.

We consider the abovementioned assumptions reasonably applicable for supporting visualization only if the simulated spatial distribution of the faculae shows similar features as the observed data. One should also bear in mind that synthetic visualization is not a proof but more an aid.

Solar faculae are generated along the AL, arbitrarily set at 0° and 180° in Carrington coordinates. This generation is accomplished through the application of a normal distribution with parameters $\mu_1 = 0$, $\sigma_1 = 25$ and $\mu_2 = 0$, $\sigma_2 = 25$, employing customary notation. The standard deviation serves as an indicator of the thickness of the AL band, as discussed in Gyenge et al. (2017). The standard deviation assumes that solar faculae originating from the AL follow a normal distribution, meaning that approximately 68% of faculae activity is now concentrated within a belt spanning $+/-25°$. The parameter μ is positioned at the center of the AL band.

The number density of AL faculae (i.e., those loci that are concentrated around the AL and are marked by red) relative to that of the rest of the faculae (marked by black) can be varied to represent localized inhomogeneity in the faculae distribution, as demonstrated in Figure 3(a). Next, let us also employ a high and low noise signal ratio to further examine their random behavior. To illustrate the impact of these high and low noise signal ratios, we used the same visualization techniques as in Figures 2 and plotted the temporal behavior of the latitude of solar faculae in Figures 3(b) and (c). The high noise signal ratio (where the signal is considered as AL) shows an easily

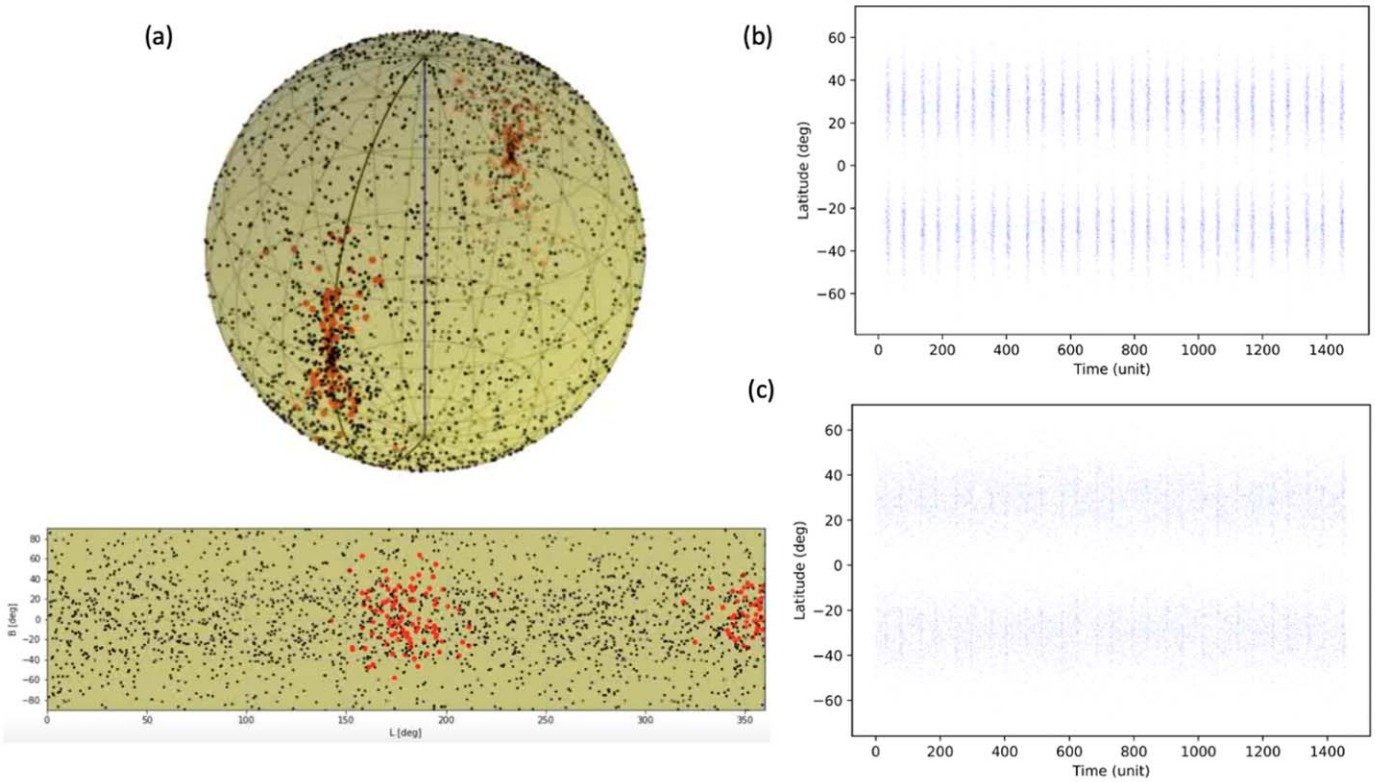

Figure 3. Panel (a): synthetic photospheric facular loci simulations depict the ALs on the Sun at an arbitrary moment in time. The upper portion of the panel presents the Sun in 3D, while the lower portion displays a 2D map of the Sun. The red dots represent the faculae located at the two ALs on the near (front) and far (rear) sides of the Sun, which are 180° apart. Black dots indicate faculae that are distributed randomly elsewhere. Panel (b) shows the spatial distribution of these simulated faculae with data enhancement marking around the AL (parallel lines) as the signal-to-noise ratio is high. Panel (c) is another example of the spatial distribution of simulated faculae data with faculae to be located randomly on the simulated surface of the Sun (parallel branches) with the signal-to-noise ratio set to an arbitrary low. An animation of panels (a) and (c) is available. The animation shows two full rotations of the synthetic photosphere and the full series in the spatial distribution. The real-time duration of the animation is 29 s.

(An animation of this figure is available.)

recognizable significant AL, as in Figure 3(b). The low signal ratio diminishes the AL; see Figure 3(c). Based on Figures 3(b) and (c), we find that this synthetic visualization modeling also demonstrates similar parallel stripes (i.e., a pair of stripes of faculae) to those found in Figure 2. This visualization modeling in Figure 3 may serve as a consistent and supporting example of aid that the observed stripes in the spatial distribution of solar faculae could be interpreted as the results of the combination of observation selection and, most importantly, the presence of AL.

We note that the synthetic visualization, just like any visualization or modeling, should not be overinterpreted. However, in this case, the simplicity speaks for itself, just as Occam's razor.

Furthermore, by investigating the spacetime display with an arbitrary strong signal ratio, also often called a time-distance diagram, crisscross patterns are revealed at the higher latitude as shown in Figure 4. These patterns are a remarkable match with those of the observed faculae data plotted in Figures 1 and 2 for latitudes between $|60°–70°|$. This finding we will now discuss in the next section.

4. The Presence of the Crisscross Pattern

We have identified regions above $|60°|$ latitudes in Figure 1(a), as also discussed in Section 3 and visualized in a simple model in Figure 4, characterized by a distinct crisscross arrangement of solar faculae, indicative of areas with increased facular density. Here, some measured properties of the crisscross patterns are reported from the southern hemisphere. There are also crisscross patterns in the northern hemisphere; however, there seem to be no hemispheric distinctions. In a zoom, Figure 5(a) illustrates the observed faculae loci with a positive magnetic field of less than 500 G at these higher latitudes, for a period with data taken between 2010 May 1 and 2011 January 1. To further analyze these patterns, we selected two arbitrary areas between latitudes of −60° and −75° in Figure 5(a). Subsequently, in Figure 5(b), we highlight these crisscross patterns using black "X" lines.

The black "X" symbols delineate zones where faculae are more densely concentrated, resulting in noticeable intersecting formations. The identification of these patterns was achieved through a systematic examination of the data plots to ensure uniformity in recognition. We determined the lifetime of each intersecting line based on how long they persisted on the time axis (horizontal x-axis), while their spatial extent was measured along the latitudinal axis (vertical y-axis). These measurements were then utilized to estimate the velocity of the facular loci patterns.

Our hypothesis is that these crisscross patterns of solar faculae loci may represent the signatures of underlying photospheric plasma motions. To explore the possible causes of these photospheric movements of faculae loci, we analyzed

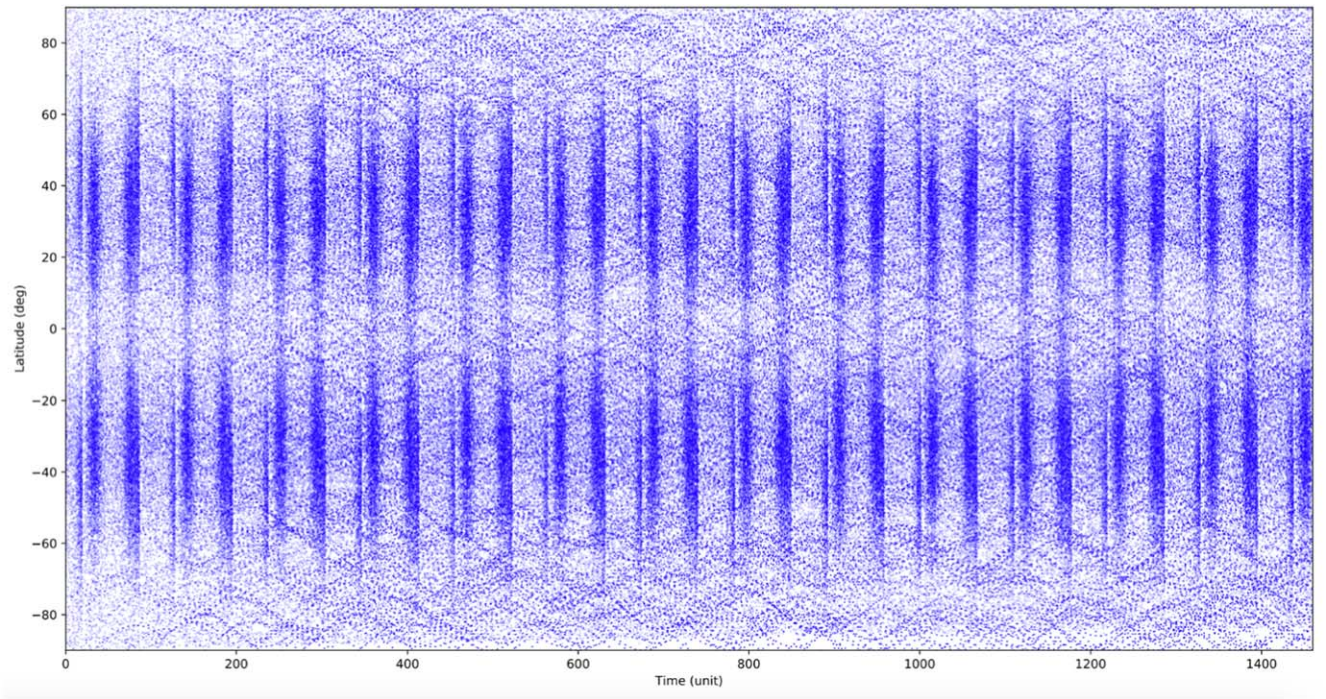

Figure 4. Scenario of the faculae distribution where a more realistic signal-to-noise ratio is applied. The model recreates all the observed features such as the parallel stripe lines and the crisscross patterns.

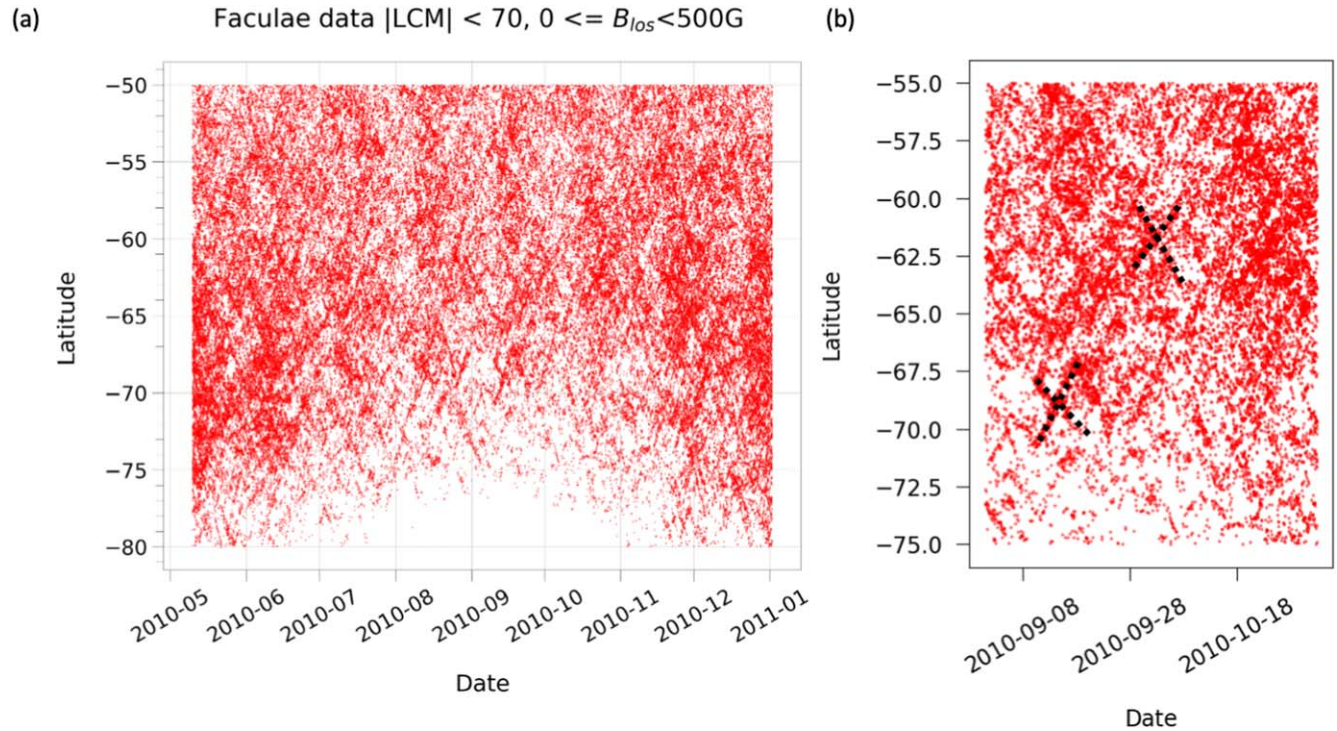

Figure 5. Panel (a): faculae distribution with positive magnetic field with values less than 500 G, between 2010 May 1 and 2011 January 1. The crisscross patterns are more observable at higher latitudes, e.g., see between $\sim -60^{\circ}$ and -75° latitudes. In panel (b), two randomly chosen typical crisscross patterns are highlighted by the black lines; however, more can be identified here.

the lifetime, spatial extent, and velocity of over 250 such patterns for the time interval from 2010 May 1 to 2014 December 31. The summary of the measured lengths and lifetimes of these crisscross patterns is depicted in Figures 6(a) and (b). From Figure 6, we infer that the crisscross patterns typically last between 30 and 130 hr, with an average duration of about 50 hr. In terms of length, these patterns are predominantly between 5 and 30 Mm, with an average length of approximately 15 Mm. From their measured lifetimes and lengths, the calculated velocity ranges between 30 and 150 m s^{-1}. Additionally, we have compiled the measured and calculated values from the year 2012 in Table 1 as an example.

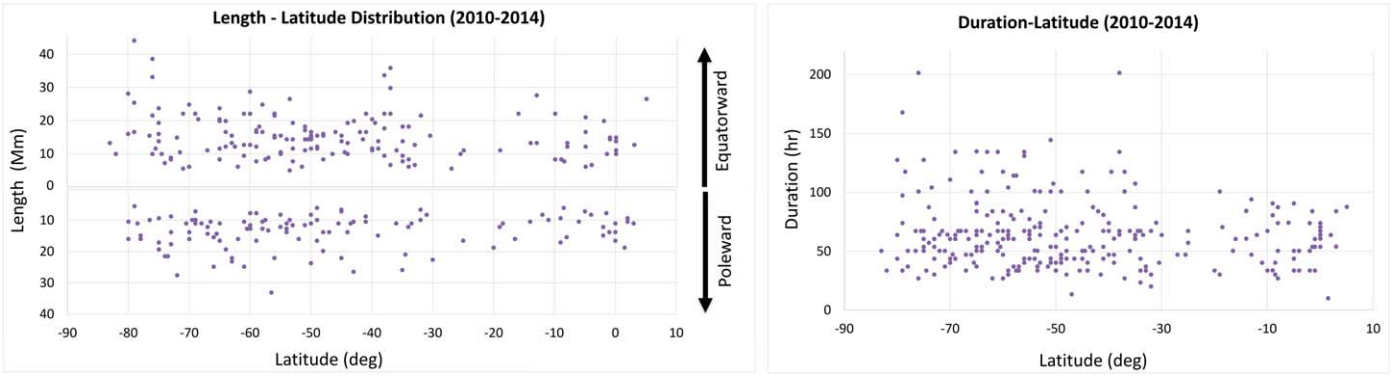

Figure 6. The figure presents the estimated values of the measured properties for crisscross pattern branches between 2010 and 2014 as a function of latitude. In panel (a), the estimated lengths of the crisscross pattern branches are depicted in Mm. The upper section of the diagram shows branches with faculae as tracers moving toward the equator, while the lower section illustrates branches heading toward the southern pole. Panel (b) displays the derived lifetimes of the crisscross patterns in hours. Some of the representative lifetimes and lengths are also given in Table 1.

Table 1
The Measured and Calculated (Estimated) Characteristic Values of Crisscross Pattern Branches for the Year 2012 in the Southern Hemisphere

2012			
Latitude	Duration (hr)	Length (km)	Velocity (m s^{-1})
−78.0	36.92	16,004.48	120.42
−80.0	63.77	16,004.48	69.71
−75.0	53.70	16,004.48	−82.79
−83.0	50.34	13,245.09	−73.08
−82.0	33.56	9933.82	−82.21
−71.0	50.34	2207.15	−121.80
−78.5	117.47	11,037.58	26.10
−75.5	67.13	11,589.45	−47.96
−43.0	50.34	19,867.64	−109.62
−45.0	50.34	6622.55	36.54
−70.0	43.63	16,004.48	101.89
−70.0	110.76	24,834.55	−62.28
−54.0	70.48	14,348.85	−56.55
−50.0	33.56	11,589.45	−95.92
−49.0	40.28	6070.67	41.87
−50.0	63.77	15,452.61	−67.31
−41.0	67.13	8830.06	36.54
−41.5	30.21	14,348.85	−131.95

Note. In the first column, the latitudes are listed. The second and third columns provide information on the measured lifetime and length, respectively. These two latter data sets are also visualized in Figure 6. The fourth column displays the derived velocities. Positive velocity values denote a poleward direction of motion (from the equator toward the southern pole), while negative velocities signify an equatorward direction of motion (from the south pole to the equator), similarly highlighted already in the case of length data in Figure 6(a).

In Table 1, positive/negative velocity values indicate the direction of poleward/equatorward motions of faculae loci, respectively, where these directions need to be considered within the plain of the time-distance plot in Figure 5. To follow the notation syntax used in dynamo simulations (see also the next section on some supporting full MHD simulations), we adopt the following. The speed is positive in the case of movement from the direction of the northern pole toward the southern one. The velocity measurements presented in the table were performed on facular loci found in the southern hemisphere, so motions toward the equator are considered with negative speeds and motions toward the southern pole are considered with positive speeds.

Based on the measured lifetimes, lengths, and velocity values, these crisscross loci patterns would be a consequence of the faculae found along the boundaries of supergranules at all latitudes (Keller et al. 2004; Priest 2014). The typical size of a supergranular cell is about 30 Mm, though it can vary from 20 to 70 Mm (Hirzberger et al. 2008; Rieutord & Rincon 2010). These sizes of supergranules are similar to our measured 5–30 Mm lengths. According to Hirzberger et al. (2008) and Nordlund et al. (2009), the evolution of a supergranule takes about half a day up to 4 days, depending on their size. For the observed facular loci, e.g., as tracers of magnetic elements, the measured lifetimes are from 30 up to 130 hr. The polar or equatorial direction of flow of a supergranule is 20–30 m s^{-1} (Rieutord & Rincon 2010), while the crisscross patterns have speeds of 30–150 m s^{-1}.

These measured values of the properties of the crisscross patterns are somewhat comparable with those of supergranular properties, suggesting that crisscross patterns may be considered to be markers of the consequences of faculae in inactive regions found along the boundaries of supergranules. The findings presented here support this conjecture and open up avenues of studying the properties of faculae as tracers to have constraints even on dynamo theory.

5. Interpretation of the Identified Properties of the Solar Faculae by MHD Simulation

The properties of faculae, like sunspots themselves, show evolution as a function of the solar cycle. For example, their loci drift poleward in contrast to sunspots' equatorward migration. More interestingly, there also exists a clear shorter-term evolutionary pattern that has a period of slightly more than a month. This shorter-term variability in the polar faculae pattern also shows a crisscross pattern (see, e.g., Figure 5).

In order to determine a plausible physical mechanism for this shorter-term spatiotemporal evolutionary pattern of the loci of faculae, we can think of the magnetohydrodynamics of the Sun's global flows and how that can influence the faculae drift pattern. One possibility is that, in polar regions, deep convection with wavenumbers one and two are favored. Gilman (1975) argued that surface convective patterns of these modes can create an overall pattern that is displaced from the rotation axis. In addition, the magnetohydrodynamic evolution of the Sun's global differential rotation and toroidal fields in

high-latitude regions show the development of $m = 1$ flow patterns with clockwise and counterclockwise swirls (see Figure 7). In both cases, the longitudinal phase speed of these nonaxisymmetric flow patterns is close to the Sun's rotation; therefore, these patterns would be like sustaining for several months in the rotating frame. Thus, the horizontal velocities could be quite large, like 100–200 m s^{-1}, and because of their nearly zero phase speed in the rotating frame, the meridional flow will appear to be reversing back and forth in the polar regions approximately every 15 days. Note that to observe such a pattern helioseismically would require averaging over 3 or 4 months; then, the residual will be much smaller and will be of the same order as an average meridional circulation, perhaps 5–10 m s^{-1}. However, 10–20 times stronger flow in a short time span can certainly exist and can impact the polar field evolution.

These swirling motions, developed due to the dynamical evolution of the Sun's differential rotation, can cause some changes in the resulting differential rotation pattern; namely, both the $m = 0$ and $m = 1$ azimuthal components of the flows can be present in the total differential rotation pattern. If the differential rotation contains only purely $m = 0$ azimuthal flow, the polar differential rotation pattern would show no tilts with respect to the polar axis. However, if the polar differential rotation pattern shows an axis tilted away from the poles, it is automatic that the differential rotation contains both $m = 0$ and $m = 1$ components. That means the meridional circulation would most likely have the same components. So, whatever $m = 0$ (axisymmetric) meridional circulation was there before the differential rotation tilted away from the polar axis, now with the tilted differential rotation, meridional circulation would contain nonaxisymmetric ($m = 1$) flows swirling in opposite directions 180° longitude apart. Thus, this would cause an addition to or subtraction from the primary axisymmetric meridional circulation pattern, depending on longitude. The addition and subtraction would create a periodically reversing component in the global meridional circulation, which can impact the transport of magnetic features, like faculae, either toward or away from the pole.

At polar latitudes, the differential rotation is weaker than at lower latitudes, so one complete rotation takes about 35 days (Finley & Brun 2023). Therefore, approximately every 35 days the reverse cell would show up. This is approximately the periodicity seen in the short-term temporal evolution of the polar faculae. If we count the number of stripes appearing around |75°| latitude in Figure 1, we find approximately 10–11 such stripes in a year.

From the above, essentially geometric, reasoning, it is possible to illustrate the approximate effect of the time-varying meridional circulation from $m = 1$ swirls in an axisymmetric flux-transport dynamo by implementing that the $m = 0$ meridional circulation is a periodic function of time, with an amplitude chosen for this periodicity determined by the angular amount the differential rotation is tilted away from the Sun's polar axis. Roughly speaking, meridional circulation would be proportional to cos(latitude) times U. The U is the linear rotational velocity at the latitude where we want to estimate meridional circulation. For example, the absolute linear rotational velocity at 60° is cos(60) times Ue, the absolute linear velocity at the equator, which is about 2 km s^{-1}. So, at 60°, it is still 1 km s^{-1}; only 10% of that 1 km s^{-1} would give rise to a relative linear rotational velocity of 100 m s^{-1}. For that, the meridional circulation at 60° would be about 50 m s^{-1}.

So, a back-and-forth appearance and disappearance of a reverse flow cell with a time of the order of 17–35 days or so can be expected. The flow speed can be as high as 100 m s^{-1} temporarily, which would be about 0–5 m s^{-1} when averaged over several months, as is done for a primary poleward flow cell at low-to-midlatitudes.

One question is, what would be a plausible mechanism to cause the tilt of the polar differential rotation away from the polar axis? If the Sun has a polar differential rotation axis that is tilted away from the long-term heliographic pole, which is historically determined by long records of sunspot rotations, then the polar regions will look as if both $m = 0$ and $m = 1$ motions are present temporarily. In that case, the rotation period of the tilted differential rotation pattern would be the period defined by the differential rotation there, as if no other effect is present.

In addition to this effect, there can be $m = 1$ Rossby waves that are propagating retrograde, with their own $m = 1$ component of flow. Figure 7 illustrates such a pattern. If the tilt away from the heliographic pole is caused by Rossby waves, then the tilt pattern would rotate with the speed of the Rossby wave. This propagation will change the period somewhat, but not substantially.

While a polar mission could give us more information about the existence of polar vortices of $m = 1$ type swirls and their influence in producing intermittent reverse flow cells, simulations of global magnetic fields' evolution in the presence of such intermittent reverse flow cells clearly indicate the crisscross type pattern in polar fields. To a rough approximation, a rotating $m = 1$ meridional circulation can be represented in an axisymmetric flux-transport dynamo by periodically reversing meridional circulation in polar latitudes. Results from such a flux-transport dynamo simulation are presented in Figure 8, in the form of a time-latitude diagram, for a case in which the reverse flow cell of amplitude 150 m s^{-1} periodically appears for a month and disappears for the entire simulation time. The numerical simulation is set up following Belucz et al. (2015), in which the primary flow cell goes up to 60° latitudes in each hemisphere, and the secondary reverse cell in each hemisphere reverses back and forth approximately every 2 weeks. While the primary (poleward) flow cell has a fixed 15 m s^{-1} maximum flow speed, the reverse (equatorward) flow cell reaches up to 150 m s^{-1} maximum flow speed in a few days and stays there for about 10 days before reversing back to be equatorward for the next 2 weeks. The turbulent diffusivity, differential rotation profile, and surface poloidal source are used as in Belucz et al. (2015).

The top panel of Figure 8 displays the butterfly diagram, which captures well the evolution of sunspot belts with about an 11 yr cycle period. The bottom panel displays the evolution of surface radial fields. If one inspects panel (b) of Figure 8, the tiny spikes above 50° latitude are visible (see these spikes in the inset box, which is enlarged on the right side of this figure). These protruding stripes in the polar fields' evolution pattern, i.e., the drift pattern with a short-term periodicity on the overall poleward migration of the radial fields, demonstrate a plausible physical mechanism for comparing with the observed faculae evolutionary pattern seen around 55° in Figure 1.

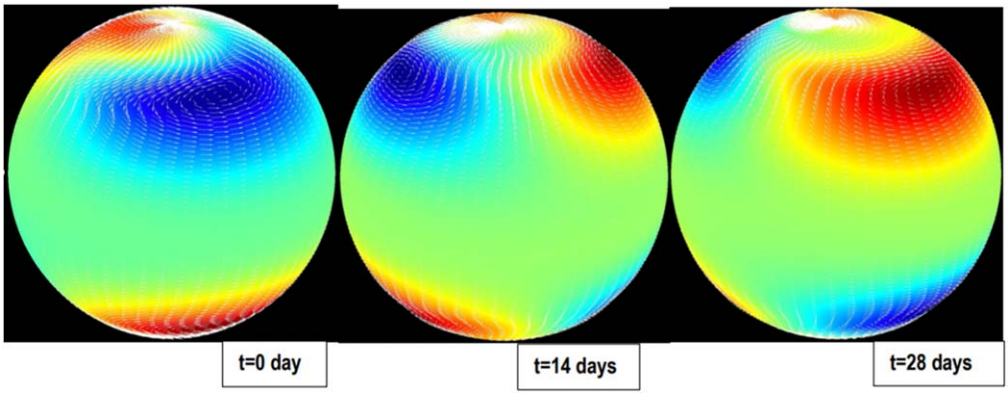

Figure 7. Three frames showing the evolution of the $m = 1$ flow pattern, clockwise in high-pressure, i.e., red regions, where the departure from hydrostatic pressure is positive and counterclockwise in low-pressure, i.e., blue regions (where the departure from hydrostatic pressure is negative). The pattern evolves slowly retrograde in longitude, due to the presence of Rossby waves.

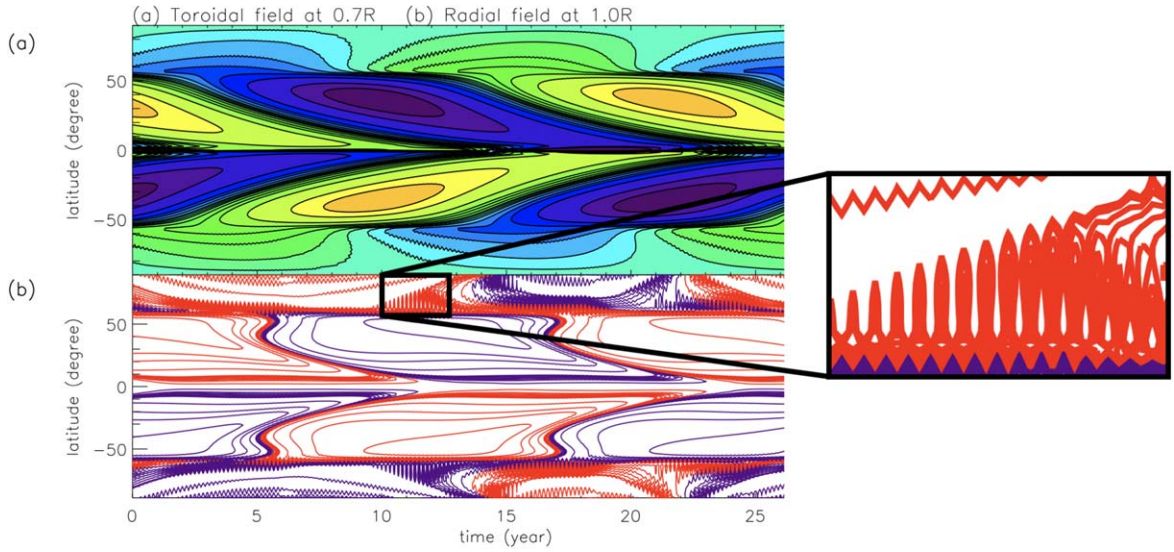

Figure 8. Time-latitude diagrams for (a) toroidal fields at the base of the convection zone and (b) radial fields at the surface, simulated with a meridional circulation having a steady primary flow but intermittently appearing and disappearing reverse flow cell periodically for about a month during the entire dynamo simulation. Protruding stripes in the polar field evolution above 50° latitude (see the zoom-in on the right in the figure) are qualitatively similar to that seen in Figure 1.

6. Periodic Behaviors of Solar Faculae

To reveal those periods in the analyzed data series of faculae loci mentioned in Sections 3 and 5, we employed a fast Fourier transform on binned 5° longitudinal segments spanning from −90° to 90° for the time interval between 2010 May 1 and 2014 December 31. For each observation, we summed the magnetic data with negative values within these 5° intervals. Note that the selection of values is arbitrary and has no bearing on the results. Subsequently, we partitioned the latitude-time diagram into 5° sections and analyzed the temporal variation of the total negative magnetic flux of faculae for each of these binned segments using the fast Fourier transform. This approach enabled us to identify dominant periods at both lower and higher latitudes, such as at 0°–5°, 5°–10°, and so on.

Based on the fast Fourier transform analysis of the summed negative magnetic field data on 5° longitudinal segments, see, e.g., Figure 9, we found a range of periods, from as long as of the order of years to a few days, that we now split into branches. Let us summarize these findings.

1. Periods are present at about 2.3, 1.5, 1.2, 0.9, 0.5–0.8, and ∼0.3 yr at all the latitude segments between −90° and 90°. Actually, these periods are identified as Rieger-type periods (110–115 days = ∼0.3 yr and 150–160 days = ∼0.4 yr by Zaqarashvili & Gurgenashvili 2018; Gurgenashvili et al. 2021) and quasi-biennial oscillations of 0.5–4 yr (Inceoglu et al. 2019). The most likely origin of the short-timescale quasiperiodicity is attributed to magnetic Rossby waves, which have periods of 0.8–2.4 yr (Dikpati & McIntosh 2020).
2. Periods with 25–30 days can also be seen at all the latitude segments between −90° and 90°. These periods relate to the differential rotation.
3. Between −45° and 45° latitude, i.e., at lower latitudes, further shorter periods were identified between 4–12 days. These periods may relate to the phenomenon and presence of AL. Interestingly, these short-term periods were also identified between the years 2010 and 2015 by Oloketuyi et al. (2019) in the time series data of low energetic solar flare classes (B- and C-class flares).

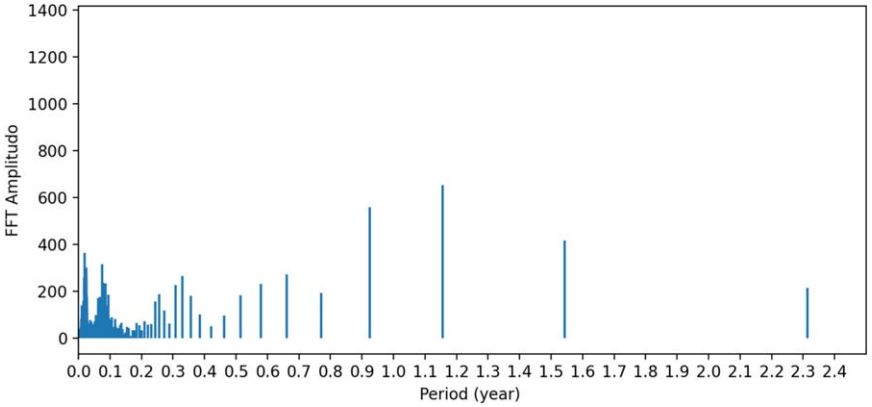

Figure 9. Fast Fourier transform of the time series of the summed negative magnetic fields of faculae loci between latitudes of 30° and 35° on the solar northern hemisphere. The periods are measured in years.

7. Conclusion

During the course of this work, we operated under the assumption that faculae are linked to the solar global subsurface magnetic fields, and their spatial and temporal distributions are considered a reflection of the broader dynamics of the evolution of global magnetic fields. We considered the faculae as surface tracers (or markers, similar to dyes in water when studying, e.g., Brownian motion) of the global magnetic fields.

We analyzed the evolution of the appearance (e.g., loci) and properties (e.g., lifetime, velocity) of solar faculae along the latitude direction in the data available between 2010 May 1 and 2014 December 31 using the Debrecen Faculae Data Catalogue (Baranyi et al. 2016). The data themselves were sampled every 2 hr within the range of −70° to 70° from the LCM, focusing on faculae with magnetic field strengths between −500 and 500 G. During the course of the analysis, we found the following, summarized for ease and transparency.

1. In Figure 1, we observe alternating strong and weak stripes at low latitudes in the spatial and temporal evolution of the loci of faculae between 2010 May 1 and 2014 December 31. These alternating stripes are consistent with a translation of approximately 10 days between the eastern and western solar limbs due to solar rotation, as illustrated in Figure 2. Namely, this 10 day interval corresponds approximately to the time it takes for a solar feature to move from LCM = −70° (on the eastern side) to LCM = 70° (on the western side). Therefore, the simplest interpretation (i.e., using Occam's razor) of the enhanced and abundant presence of faculae visualized as these alternating stripes is associated with the debated conjecture of the presence of the AL, i.e., a branch of longitudinal loci where sunspots, photospheric faculae, and other solar activity tend to concentrate or reoccur over time. We supported this hypothesis using a simple synthetic (kinetic) model, which is consistent with and confirmed the relationship between the alternating stripes and the concept of AL. For more details, please refer back to Section 3.
2. In addition, intriguing crisscross patterns were observed at higher latitudes, specifically at ±60° and ±75°, as shown, e.g., in Figure 5. We measured and analyzed the lifetime, length, and velocity of over 250 of these crisscross patterns in the time interval between 2010 May 1 and 2014 December 31. Based on their characteristics, we conjecture that these crisscross patterns may result from the presence of faculae in magnetically inactive regions found along the boundaries of supergranules at all latitudes (Keller et al. 2004; Priest 2014). Based on the study by Schou (2003), the meridional flow appears to be reliably measurable between ±75° latitudes, which also supports that these crisscross patterns are not present because of the foreshortening at higher latitudes.

   Supergranules typically have a size of about 30 Mm, but this can vary from 20 to 70 Mm (Hirzberger et al. 2008; Rieutord & Rincon 2010). These characteristic sizes are similar to the length values we obtained for the observed crisscross patterns, which range from 5 to 30 Mm.

   Further, according to Hirzberger et al. (2008) and Nordlund et al. (2009), the evolution of a supergranule may take from half a day up to 4 days, depending on its size. We found lifetimes of the crisscross patterns ranging from 30 to 130 hr.

   Additionally, the vertical (i.e., polarward) flow of a supergranule is typically around 20–30 m s^{-1} (Rieutord & Rincon 2010), while the crisscross patterns represent velocities ranging from 30 to 150 m s^{-1}. The two velocity ranges are somewhat comparable (e.g., their order of magnitude), but the agreement is not perfect, and this may require further analyses. Therefore, this conclusion should remain as a conjecture.
3. Last but not least, we were able to identify various oscillations in the loci of the facula data set. First, the solar quasi-biennial oscillations (ranging from 0.3 to 2 yr) were prominently present in the time series records of latitudinally binned (5° is a bin) solar faculae observed between 2010 May 1 and 2014 December 31. Specifically, we measured periods—listed in decreasing order—of 2.3, 1.5, 1.2, 0.9, 0.5–0.8, and ∼0.3 yr across the −90° to 90° latitude range. These findings align well with the dynamo simulations we carried out and described in Section 5.

   However, furthermore, we also identified shorter periods of 4–12 days between −45° and 45°, i.e., at lower latitudes. These periods are suggested to be strongly related to the existence of ALs, as discussed in Section 3. These short-term periods had previously also been observed between 2010 and 2015 by, e.g., Oloketuyi et al. (2019) in the time series of low-energy solar flare classes. This correlation adds an intriguing layer of consistency and support to our findings.

Based on the above results and employing faculae, abundantly present in the lower solar atmosphere, as tracers or markers of subsurface dynamics, we found that faculae tend to cluster around active regions, exhibiting a nonaxisymmetric longitudinal distribution similar to that of sunspots.

Our data and findings show that the longitudinal spatial distribution of faculae remains unaffected by the continuous drift caused by the differential rotation, as indicated by the identification of the observed AL. This may suggest that faculae observed in AL regions are likely situated close to strong magnetic field line branches rooted near the tachocline, thereby evading the effects of differential rotation. If this holds true, it implies the presence of a nonaxisymmetric dynamo process.

Other potential explanations include a relic field misaligned from the rotational axis or the dipole field with a differential angular rotation distinct from that of the Sun. It is also possible that the dynamo itself generates and stores fields, nonreversing for a much longer time than the decadal solar cycle, more like at century or millennium timescales (Mestel & Weiss 1987; Dikpati et al. 2006). There is recent observational evidence for long-term asymmetries in the solar poloidal fields that suggest a component of the field is not reversing with each new solar cycle (Mursula 2023).

Further research is needed to validate these assumptions and refine our understanding of faculae and their relationship to the Sun's global magnetic field. Future potential missions may further confirm or refute some details of our present views on this topic.

Acknowledgments

E.E., M.B.K., N.G.Y., B.B., and R.E. acknowledge support from the European Union's Horizon 2020 research and innovation program under grant agreement Nos. 739500 (PRE-EST project) and 824135 (SOLARNET project). R.E. and M.B.K. are also thankful for the support received from NKFIH OTKA (Hungary, grant No. K142987) and the ISSI-Beijing program "Step forward in solar flare and coronal mass ejection (CME) forecasting". R.E. is grateful to STFC (UK, grant No. ST/M000826/1) and PIFI (China, grant No. 2024PVA0043). M.B.K. acknowledges support by the Universita' degli Studi di Catania (PIA.CE.RI. 2020–2022 Linea 2), by the Italian MIUR-PRIN grant 2017APKP7T, CAESAR ASI-INAF n. 2020-35-HH.0 project and ÚNKP-23-4-II-ELTE-107, ELTE Hungary. B.B.'s work is supported by the Newton International Fellowship of the Royal Society, program No. NIF-R1-192417. M.D. acknowledges support from the National Center for Atmospheric Research, which is a major facility sponsored by the National Science Foundation under cooperative agreement 1852977. M.D. also acknowledges partial support from several NASA grants—NASA-LWS award 80NSSC20K0355 and NASA-HSR award 80NSSC21K1676 awarded to NCAR and also two subawards from JHU/APL's NASA-HSR grant with award No. 80NSSC21K1678 and from Stanford's COFFIES Phase II NASA-DRIVE Center with award No. 80NSSC22M0162. N.G.Y. acknowledges the NVIDIA Academic Hardware grant program for their support, providing essential computational resources (NVIDIA A5000 GPU).

ORCID iDs

Anett Elek https://orcid.org/0000-0003-3379-0988
Marianna B. Korsós https://orcid.org/0000-0002-0049-4798
Mausumi Dikpati https://orcid.org/0000-0002-2227-0488
Norbert G. Gyenge https://orcid.org/0000-0003-0464-1537
Bernadett Belucz https://orcid.org/0000-0002-0040-1790
Robertus Erdélyi https://orcid.org/0000-0003-3439-4127

References

Baranyi, T., Győri, L., & Ludmány, A. 2016, SoPh, 291, 3081
Belucz, B., Dikpati, M., & Forgács-Dajka, E. 2015, ApJ, 806, 169
Benevolenskaya, E. E., Hoeksema, J. T., Kosovichev, A. G., & Scherrer, P. H. 1999, ApJL, 517, L163
Berger, T. E., Title, A. M., Tarbell, T., et al. 2007, in ASP Conf. Ser. 369, New Solar Physics with Solar-B Mission, ed. K. Shibata, S. Nagata, & T. Sakurai (San Francisco, CA: ASP), 103
Bumba, V., & Howard, R. 1969, SoPh, 7, 28
Castenmiller, M. J. M., Zwaan, C., & van der Zalm, E. B. J. 1986, SoPh, 105, 237
Chapman, G. A., Cookson, A. M., & Dobias, J. J. 1997, ApJ, 482, 541
Charbonneau, P. 2020, LRSP, 17, 4
de Toma, G., White, O. R., & Harvey, K. L. 2000, ApJ, 529, 1101
Dikpati, M., & Charbonneau, P. 1999, ApJ, 518, 508
Dikpati, M., Gilman, P. A., & MacGregor, K. B. 2006, ApJ, 638, 564
Dikpati, M., & McIntosh, S. W. 2020, SpWea, 18, e02109
Elek, A., Gyenge, N., Korsós, M. B., & Erdélyi, R. 2017, in IAU Symp. 335, Space Weather of the Heliosphere: Processes and Forecasts (Cambridge: Cambridge Univ. Press), 17
Finley, A. J., & Brun, A. S. 2023, A&A, 674, A42
Foukal, P. 1998, ApJ, 500, 958
Foukal, P., & Lean, J. 1986, ApJ, 302, 826
Frazier, E. N. 1971, SoPh, 21, 42
Gaizauskas, V., Harvey, K. L., Harvey, J. W., & Zwaan, C. 1983, ApJ, 265, 1056
Gilman, J. J. 1975, JAP, 46, 5110
Gurgenashvili, E., Zaqarashvili, T. V., Kukhianidze, V., et al. 2021, A&A, 653, A146
Gyenge, N., Baranyi, T., & Ludmány, A. 2014, SoPh, 289, 579
Gyenge, N., Ludmány, A., & Baranyi, T. 2016, ApJ, 818, 127
Gyenge, N., Singh, T., Kiss, T. S., Srivastava, A. K., & Erdélyi, R. 2017, ApJ, 838, 18
Győri, L. 2012, SoPh, 280, 365
Haigh, J. D. 2007, LRSP, 4, 2
Hale, G. E. 1922, MNRAS, 82, 168
Hirayama, T. 1978, PASJ, 30, 337
Hirzberger, J., Gizon, L., Solanki, S. K., & Duvall, T. L. 2008, SoPh, 251, 417
Homann, T., Kneer, F., & Makarov, V. I. 1997, SoPh, 175, 81
Hovis-Afflerbach, B., & Pesnell, W. D. 2022, SoPh, 297, 48
Inceoglu, F., Simoniello, R., Arlt, R., & Rempel, M. 2019, A&A, 625, A117
Janssens, J. 2021, JSWSC, 11, 3
Keller, C. U., Schüssler, M., Vögler, A., & Zakharov, V. 2004, ApJL, 607, L59
Mandal, S., Chatterjee, S., & Banerjee, D. 2017, ApJ, 835, 62
Mestel, L., & Weiss, N. O. 1987, MNRAS, 226, 123
Muñoz-Jaramillo, A., Sheeley, N. R., Zhang, J., & DeLuca, E. E. 2012, ApJ, 753, 146
Mursula, K. 2023, A&A, 674, A182
Nordlund, R. F., Stein, K., & Asplund, M. 2009, LRSP, 6, 2
Oloketuyi, J., Liu, Y., & Zhao, M. 2019, ApJ, 874, 20
Parker, E. N. 1955, ApJ, 122, 293
Priest, E. 2014, Magnetohydrodynamics of the Sun (Cambridge: Cambridge Univ. Press)
Priyal, M., Banerjee, D., Karak, B. B., et al. 2014, ApJL, 793, L4
Rieutord, M., & Rincon, F. 2010, LRSP, 7, 2
Ruždjak, D., Brajša, R., Skokić, I., Sudar, D., & Hanslmeier, A. 2023, SoPh, 298, 39
Schou, J. 2003, ApJL, 596, L259
Shapiro, A. I., Solanki, S. K., Krivova, N. A., et al. 2014, A&A, 569, A38
Sheeley, N. R. 1991, ApJ, 374, 386
Sheeley, N. R. 2008, ApJ, 680, 1553
Solov'ev, A. A., & Kirichek, E. A. 2019, MNRAS, 482, 5290
Spruit, H. 1976, SoPh, 50, 269
Spruit, H. C. 1977, SoPh, 55, 3
Title, A. M., Topka, K. P., Tarbell, T. D., et al. 1992, ApJ, 393, 782
Tlatov, A. G. 2009, SoPh, 260, 465
van Driel-Gesztelyi, L., & Green, L. M. 2015, LRSP, 12, 1
Walton, S. R., Preminger, D. G., & Chapman, G. A. 2003, ApJ, 590, 1088
Yeo, K. L., Krivova, N. A., & Solanki, S. K. 2014, SSRv, 186, 137
Yeo, K. L., Solanki, S. K., Norris, C. M., et al. 2017, PhRvL, 119, 091102
Zaqarashvili, T. V., & Gurgenashvili, E. 2018, FrASS, 5, 7